NSRRC-J04393 (2014)

Journal of Materials Chemistry B

COMMUNICATION

View Article Online
View Journal | View Issue

Published on 12 June 2014. Downloaded by National Tsing Hua University on 29/07/2014 02:52:51.

Cite this: J. Mater. Chem. B, 2014, 2, 4988

Received 13th May 2014
Accepted 11th June 2014

DOI: 10.1039/c4tb00771a

www.rsc.org/MaterialsB

pH-responsive hierarchical transformation of charged lipid assemblies within polyelectrolyte gel layers with applications for controlled drug release and MR imaging contrast†

Yi-Fong Huang,[a] Wen-Hsuan Chiang,[b] Wen-Chia Huang,[b] Hsin-Hung Chen,[a] Ming-Yin Shen,[bc] Sung-Chyr Lin,[a] Chorng-Shyan Chern[d] and Hsin-Cheng Chiu*[b]

A cationic lipid-embedded poly(acrylic acid) (PAAc) gel layer coated on chitosan/superparamagnetic iron oxide nanoparticle (SPION) nanohybrid surfaces effectively modulates drug release and MR imaging contrast by pH-responsive morphological transformation and hierarchical alignment of the lipid assemblies.

The great potential of nanoscale delivery systems of bioactive agents for cancer therapeutics and diagnostics demonstrated in the past decade comes mostly from the feasibility of imparting pertinent stimuli-responsive properties to the systems and the local accumulation of nanoparticles within tumors.[1–4] While the latter is intimately associated with the facilitated extravasation and enhanced residence of nanoscale structures within tumor tissue (*i.e.*, the enhanced permeability and retention effect), the former enhances the therapeutic/diagnostic performance in a well controlled manner. This is mainly achieved *via* the delicate design in structural/morphological response to external or internal stimuli. Polymeric assemblies (*e.g.*, micelles and vesicles) from intermolecular packing of block or graft amphiphilic copolymers have been one of the primary interests in nanomedicine applications owing to their controllable responses in supramolecular architectures to environmental stimuli.[5–10] Taking advantage of the structural response to external stimuli (*e.g.*, temperature, pH, light and voltage), polymeric vesicles could achieve selective delivery/release of small drugs, proteins, genes and diagnostic probes.[5–10] For example, pH-responsive micelles from assembly of the block copolymer of poly(ethylene glycol) (PEG) and cholic acid-conjugated poly(*N*-(*N*′,*N*′-diisopropylaminoethyl) aspartamide) (PAsp(DIP)) in aqueous solution of pH 7.4 were developed for co-delivery of paclitaxel molecules and quantum dots to tumor tissues.[5] Through the acid-induced protonation and dissolution of the PAsp(DIP) interlayer at low pH, drug species were released promptly. The voltage-responsive vesicles could be attained by the orthogonal assembly of poly(styrene)-β-cyclodextrin and PEG–ferrocene in aqueous solution *via* terminal host–guest interactions.[8] The reversible association and disassociation of polymeric vesicles and the liberation of entrapped cargoes can be remotely controlled by alteration of applied voltage strength.

It should be noted that most copolymers used to fabricate stimuli-responsive polymeric assemblies require rather complicated chemical processes along with the use of toxic reagents and organic solvents, thereby severely limiting their practical applications in the biomedical field. To address this issue, it is essential to design a facile and reproducible approach to prepare a drug delivery system comprising polymeric assemblies with desirable stimuli-responsive properties. In our previous work,[11] pH-responsive hybrid nanovesicles were readily obtained by spontaneous co-assembly of poly(acrylic acid) (PAAc)-*g*-monomethoxy poly(ethylene glycol) (mPEG) with a cationic lipid, didodecyldimethylammonium bromide (DDAB), in an aqueous solution of pH 8.9 *via* electrostatic interaction. With the solution pH being reduced to 5.0, unionized AAc-rich transmembrane channels were formed at locations near mPEG coronas because of the significant disruption of consecutive ionic pairings of DDAB species with PAAc segments in the vesicle membrane with the aid of the presence of extremely hydrated and mobile mPEG chains extending into the aqueous phase. The greatly promoted release of the encapsulated therapeutic payload can then be achieved. In this work, the lipid-embedded polyelectrolyte gel surface layer (serving as a pH-controllable molecular valve-like device) surrounding a magnetic core particle was developed. This unique device was achieved simply by the morphological transformation and hierarchical alignment of cationic lipid

[a]Department of Chemical Engineering, National Chung Hsing University, Taichung 402, Taiwan

[b]Department of Biomedical Engineering and Environmental Sciences, National Tsing Hua University, Hsinchu 300, Taiwan. E-mail: hscchiu@mx.nthu.edu.tw

[c]Department of Surgery, National Taiwan University Hospital-Hsinchu Branch, Hsinchu 300, Taiwan

[d]Department of Chemical Engineering, National Taiwan University of Science and Technology, Taipei 106, Taiwan

† Electronic supplementary information (ESI) available: Experimental details and further characterization of the folate-decorated lipid/gel-coated CSN_{DOX}. See DOI: 10.1039/c4tb00771a

This journal is © The Royal Society of Chemistry 2014

Published on 12 June 2014. Downloaded by National Tsing Hua University on 29/07/2014 02:52:51.

assemblies within the thin PAAc gel layer. 1,2-Dioleoyl-3-trimethylammonium-propane (DOTAP) was used to demonstrate the lipid hierarchical assembly in response to changes in environmental pH in this study. Small angle X-ray scattering (SAXS) patterns showed that sphere-like DOTAP micelles inside the PAAc-constituting gel layer at pH 7.4 underwent morphological transformation upon acid-triggered reduction in both ionization of AAc residues and charge binding with DOTAP species. This led to re-assembly of DOTAP species into rod-like structures (for example, at pH 6.0) and hierarchical packing into disk-like aggregates (at pH 5.4) (Fig. 1). Concomitantly, due to the significant change of electrostatic interaction of DOTAP species in different assembly structures with the AAc residues of the gel layer, the cross-linking density of the gel layer varies, thereby leading to permeability regulation of the gel layer to water molecules as well as to the therapeutic payload.

To demonstrate the capability of hierarchical lipid assembly structures in controlling the gel permeability, the cross-linked polyelectrolyte gel layer laden with both DOTAP and doxorubicin (DOX; an anticancer agent) was coated onto the organic/inorganic hybrid nanosphere. The template particles were prepared by coassembly of chitosan with citric acid-modified superparamagnetic iron oxide nanoparticles (SPIONs; *ca.* 8–10 nm in diameter, Fig. S1a†) *via* electrostatic interaction. To prevent the gel-coated particles from aggregation at low pH, they were further stabilized by ω-cholesterol-PEG-folate *via* the steric stabilization effect. Note that the cholesterol moiety was used as an anchor, and folate was used as a targeting ligand in nanomedicine applications. The schematic representation of the particle morphology is illustrated in Fig. 1. The preparation of citric acid-conjugated SPIONs, chitosan/SPION (CSN) templates, ω-cholesterol-PEG (M_w 2000 g mol^{-1})-folate, and DOTAP/DOX-laden gel-coated nanoparticles is described in detail in the ESI.† The template particles have a mean hydrodynamic diameter (D_h) of *ca.* 70 nm and a relatively uniform particle size distribution (polydispersity index (PDI) 0.21) (Table 1). Distinct from the zeta potential of the citric acid-covered SPION alone (−24 mV at pH 5.0), the zeta potential of CSN was changed from −24 to +35 mV. This confirms the formation of hybrid complexes surrounded by positively charged chitosan chain segments for the template particles. After being caged with the PAAc gel layer at pH 6.0, the particles were enlarged to *ca.* 91 nm. They further grew to 120 nm after drug loading at pH 7.4. With cationic DOTAP species being embedded, the particle size became rather invariant in response to changes in pH, yet the surface charge density, as reflected in the zeta potential data, remained strongly pH dependent (Table 1 and Fig. S5†). It is also interesting to note that the polyelectrolyte gel can endow CSN with a more robust structure to resist the large-volume dilution with phosphate buffered saline (PBS) (Fig. S6†). TEM images of gel-caged nanoparticles clearly illustrate the spherical morphology and verify the successful deposition of PAAc-based gel onto the template particle surface (Fig. S1b and c†).

Through simple incorporation of DOTAP species with a preset weight ratio (*e.g.*, W_{DOTAP}/W_{PAAc} = 0.25 (w/w)) into the aqueous gel-caged CSN dispersion at pH 7.4, lipid assemblies were readily developed within the PAAc-constituting outlayered gel phase. The resultant particles showed an appreciable increase in the particle size and a slight reduction in the zeta potential yet retained a mono-modal particle size distribution (Table 1 and Fig. S5†). The TEM image also verifies the essentially unchanged particle morphology after incorporating DOTAP into the gel layer (Fig. S1d†). Obviously, DOTAP species became mostly embedded inside the gel layer that thus enlarged the surface layer dimension. At pH 7.4, at which the AAc residues were mostly deprotonated, the amphiphilic DOTAP molecules within the gel layer underwent hydrophobically-driven assembly *via* their nonpolar tails while the positively charged head groups being associated with the ionized AAc residues *via* electrostatic interaction. The pH-evolved variation of the interaction of DOTAP molecules with ionized AAc residues and the subsequent structural rearrangement of the DOTAP assembly and the potential applications in nanomedicine are the major foci to be explored in this study.

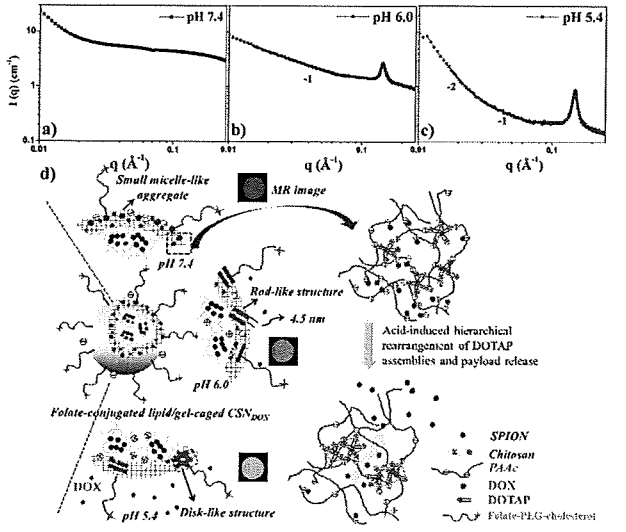

Fig. 1 SAXS profiles of the lipid/gel-caged CSN in aqueous solution at (a) pH 7.4, (b) 6.0 and (c) 5.4. (d) Schematic illustration of the pH-triggered structural transition of DOTAP aggregates in the gel layer of the lipid/gel-caged CSN with controlled drug release and MR imaging contrast.

Table 1 Mean hydrodynamic diameters (D_h), polydispersity indices (PDI) and zeta potential values of hybrid nanoassemblies in aqueous solutions at 25 °C

Sample	pH	D_h (nm)	PDI	ζ-potential (mV)
CSN	5.0	70 ± 4	0.21	35 ± 2
Gel-caged CSN	6.0	91 ± 3	0.15	−36 ± 3
	7.4	101 ± 4	0.17	−46 ± 2
Lipid/gel-caged CSN	7.4	120 ± 3	0.16	−39 ± 4
	5.4	123 ± 3	0.16	−24 ± 4
Lipid/gel-caged CSN$_{DOX}$	7.4	120 ± 4	0.15	−39 ± 2
FA-conjugated lipid/gel-caged CSN$_{DOX}$	7.4	119 ± 3	0.17	−20 ± 2

Published on 12 June 2014. Downloaded by National Tsing Hua University on 29/07/2014 02:52:51.

The effects of medium pH on the primary molecular packing architecture of DOTAP species and the secondary assembly alignment within the gel surface layer surrounding the CSN template were studied mainly by SAXS. As revealed in Fig. 1a, the scattering profile of lipid/gel-coated CSN at pH 7.4 shows the absence of any characteristic Bragg peaks. Considering such a high level of lipid being accommodated within the gel layer, it is most likely that the resultant lipid assembly exhibits a spherical micelle-like structure (*ca.* 3.2 nm in radius as estimated by the spherical micelle modeling fit) characterized by the lack of regular lamellar arrangement, as evidenced by SAXS measurements. Nonpolar tails of DOTAP species self-associate with one another to form the hydrophobic core. In the meantime, the cationic head groups located within the micellar shell electrostatically interact with the ionized AAc units of the gel phase. As a result, lipid micelles reside randomly throughout the gel layer and act as additional effective cross-linking junctions by connecting themselves with PAAc chain segments *via* the charge interaction. This will then lead to an increase in the cross-linking density of the gel phase. The schematic illustration of lipid micelles acting as the cross-linking points within the nanogel layer is shown in Fig. 1d.

When the medium pH is lowered from 7.4 to 6.0, the SAXS profile of the lipid/gel-caged CSN exhibits a sharp Bragg peak with an interlamellar d spacing ($2\pi/q$) of *ca.* 4.5 nm at $q = 0.14$ Å^{-1}. The scattering intensity decay perfectly matches the power law dependence of q^{-1} ($\alpha = 1$) in the q region 0.03–0.06 Å^{-1}. This strongly suggests the development of rod-like DOTAP micelles (with *ca.* 3.9 nm and 9.1 nm in radius and length, based on the cylinder modeling fit), which closely align to each other with a d spacing of 4.5 nm (Fig. 1b). Similar SAXS observations on the rod-like micelle structure in simple aqueous phases have been reported elsewhere.[12–14] This is primarily due to the reduced negative charges within the gel layer and, consequently, the decreased electrostatic interaction of the AAc residues with DOTAP species. Under the circumstances, the morphological transformation of DOTAP micelles into a rod-like structure and inter-assembly alignment occurs. With the medium pH being further reduced to 5.4, the SAXS profile was well fitted to the power law dependence of q^{-1} in the higher q range (0.03–0.06 Å^{-1}) and q^{-2} in the lower range (0.012–0.025 Å^{-1}), respectively (Fig. 1c). Such a scattering pattern illustrates the formation of disk-like lipid aggregates within the AAc-rich gel layer, which is in line with the single particle form factor ($\alpha = 2$) of a disk in the low q region.[12,15,16] According to the q^{-1} dependence in the q range 0.03–0.06 Å^{-1}, the plate structure formed primarily by enhanced stacking of primary rod-like lipid assemblies into such a secondary-level architecture. Such a hierarchical alignment also resulted in a slight reduction in d-spacing from 4.5 to 4.2 nm. In view of the absence of morphological response of DOTAP assemblies dispersed in water to changes in pH (data not shown), the pH-evolved morphological transformation from the spherical to the rod-like structure and subsequent hierarchical alignment of the primary rod-like structure into the secondary plate structure are controlled virtually by the degree of ionization of the AAc residues and charge binding of the AAc units with DOTAP species in the gel layer (Fig. 1d). This inevitably leads to an increase in the size of individual DOTAP aggregates and a decrease in the extent of physical cross-links.

Fig. 2a shows that, in the absence of DOTAP, the cumulative release of DOX from gel-coated CSN is rather fast and uncontrollable, more than 80% over a period of 12 h at either pH 7.4 or 5.4 ($I = 0.15$ M). With DOTAP being embedded in the gel layer ($W_{DOTAP}/W_{PAAc} = 0.25$ (w/w)), the drug unloading at pH 7.4 was largely retarded. Nevertheless, the response in drug release to changes in pH in the range 7.4–5.4 is significantly enlarged. Fig. 2b shows the influence of the level of DOTAP incorporated into the gel layer on the drug release at pH 7.4 (or 5.4) over a period of 12 h. Note that the drug release ratio, defined as the ratio of the cumulative drug release at pH 5.4 to that at pH 7.4 over a period of 12 h, was used as a quantitative pH-responsive unloading index in this work. Although the drug release at pH 7.4 (or 5.4) decreases with increasing the level of DOTAP, the pH-responsive unloading index reaches a maximal value at the weight ratio (W_{DOTAP}/W_{PAAc}) of 0.25. Obviously, accommodation of DOTAP within the outlayered gel at such an optimal level can

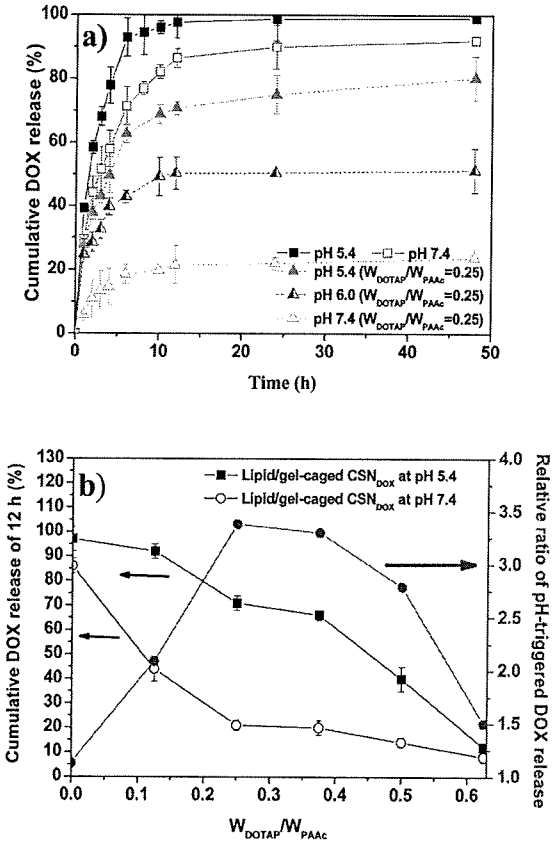

Fig. 2 (a) Time evolution of cumulative drug release for the gel-caged CSN_{DOX} (squares) and lipid/gel-caged CSN_{DOX} (triangles) in aqueous solutions of different pH at 37 °C. (b) Cumulative drug release of the lipid/gel-caged CSN_{DOX} with different weight ratios of DOTAP to PAAc (W_{DOTAP}/W_{PAAc}) at pH 5.4 and 7.4 over a period of 12 h. The profile of the ratio of the cumulative drug release at pH 5.4 to that at 7.4 as a function of W_{DOTAP}/W_{PAAc} is also included.

This journal is © The Royal Society of Chemistry 2014

Published on 12 June 2014. Downloaded by National Tsing Hua University on 29/07/2014 02:52:51.

effectively prevent DOX from prematurely leaking at pH 7.4 while desirable drug unloading at mildly acidic pH can be achieved. Compared with the lipid-free case, the pH-induced hierarchical rearrangement of DOTAP assemblies within the PAAc gel layer is obviously the root cause for the delicate regulation of DOX release (Fig. 1d). At pH 7.4, the cross-linking density of the gel layer is greatly enhanced as a result of the presence of spherical micelles of DOTAP in a large quantity, which serve as additional cross-link junctions. With the medium pH being reduced from 7.4 to 5.4, transformation of primary spherical assemblies of DOTAP into a rod-like structure and subsequent hierarchical alignment of the rod-like structure into the secondary plate architecture occur in the gel layer. Thus, the cross-linking density of the gel layer is significantly reduced, which in turn facilitates drug efflux.

SPIONs have been extensively exploited as a theranostic system in MR imaging, hyperthermia and magnetic guidance.[17–20] Fig. 3a shows that the lipid/gel-caged CSN at pH 5.4 exhibits an appreciably higher r_2 value as compared to either citric acid-coated SPION or CSN alone. The parameter r_2 is the slope of the straight line passing through the relaxation rate ($1/T_2$) *vs.* Fe concentration data points. Obviously, it is the high water-retaining capacity of the lipid-embedded gel layer surrounding CSN that is responsible for the enhanced MR imaging contrast. This is achieved by prolonging the acting time of water molecules in the CSN generated magnetic field.[21,22] With the pH being raised from 5.4 to 7.4, the r_2 value of the lipid/gel-coated CSN_{DOX} is considerably increased from 183 to 252 mM^{-1} s^{-1} in contrast to the minor pH effect on r_2 for undecorated SPION. This is ascribed largely to the restrained spatial motion of the interior CSN, which originates from the pH-evolved reinforcement of the cross-linking density of the gel layer in addition to the enhanced SPION clustering as a result of the reduced protonation of chitosan chain segments (Fig. 1d). Again, the pH-triggered transformation and hierarchical alignment of lipid assemblies within the gel layer are the root causes. The pH-responsive T_2-weighted MR imaging illustrated in Fig. 3b is in good agreement with the observed r_2 values as a function of pH. Thus, the DOTAP-embedded polyelectrolyte gels show great potential to promote the pH-responsive MR imaging contrast and to be used to detect the pH of malignant tumoral microenvironments closely related to the resistance to cancer treatment and the mortal phenotype of cancer sickness.[2,23,24] Additional *in vitro* evaluation of the entire folate (FA)-decorated lipid/gel-coated CSN_{DOX} as an effective theranostic delivery system was performed. The folate-decorated lipid/gel-caged CSN_{DOX} has been found capable of remarkably enhancing intracellular DOX fluorescence intensity and T_2-weighted MR image contrasts compared to the folate-free counterpart (Fig. S8a†). With the appreciable deposition of DOX species in cell nuclei (Fig. S8b†), the result also verifies effective drug release of the lipid/gel-coated CSN_{DOX} from acidic endosomes/lysosomes which is most likely achieved with the aid of the structural switch of lipid assemblies. More details are included in the ESI.†

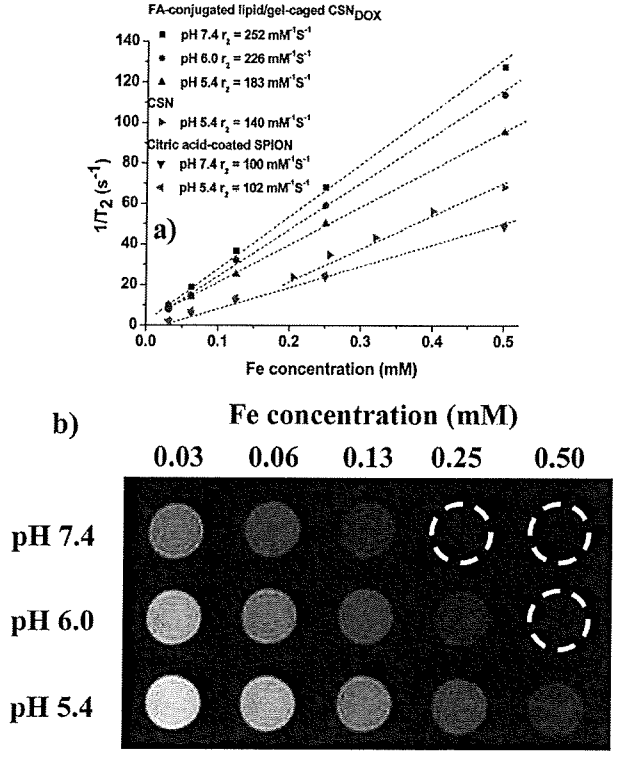

Fig. 3 (a) Reciprocal of T_2 (relaxation rate) as a function of Fe concentration for CSN at pH 5.4, folate-conjugated lipid/gel-caged CSN_{DOX} and citric acid-coated SPION at different pH. (b) T_2-weighted MR images of the folate-conjugated lipid/gel-caged CSN_{DOX} at different pH.

In summary, we have developed an outer PAAc-constituting gel layer, which is capable of modulating payload release and MR imaging contrast simply by embedding cationic DOTAP species within the gel layer. The DOTAP assemblies inside the gel layer undergo morphological transformation from sphere to rod-like micelles and subsequent hierarchical alignment into disk-like stacking in response to regulated electrostatic interactions of DOTAP species with AAc residues when the medium pH changes from 7.4 to 5.4. Taking advantage of the structural switch of lipid assemblies as a control valve, the PAAc gel coated on the CSN surface can greatly retard premature payload efflux at pH 7.4, yet retain satisfactory cargo release at pH 5.4. With the medium pH being adjusted, changes in both the gel structure and protonation of chitosan chain segments lead to a highly pH-controllable MRI contrast. This work demonstrates that combining the lipid-embedded polyelectrolyte gel surface layer with a magnetic core particle shows great potential to achieve effective cancer theranostics.

Acknowledgements

This work is supported by the National Science Council (NSC 102-2221-E-007-032-MY3 and NSC 102-2221-E-007-133-MY3), National Tsing Hua University (101N7046E1) and National Taiwan University Hospital-Hsinchu Branch (HCH103-036). The authors also thank the National Synchrotron Radiation Research Center (Hsinchu, Taiwan) for the use of SAXS (23A1) and the 7T animal MRI Core Lab of the Neurobiology and

Cognitive Science Center for technical and facility supports, and the Instrumentation Center for MRI experiments conducted at National Taiwan University.

Notes and references

1 W. H. Chiang, V. T. Ho, W. C. Huang, Y. F. Huang, C. S. Chern and H. C. Chiu, *Langmuir*, 2012, **28**, 15056–15064.
2 J. Y. Ko, S. Park, H. Lee, H. Koo, M. S. Kim, K. Choi, I. C. Kwon, S. Y. Jeong, K. Kim and D. S. Lee, *Small*, 2010, **6**, 2539–2544.
3 S. M. Lee, Y. Song, B. J. Hong, K. W. MacRenaris, D. J. Mastarone, T. V. O'Halloran, T. J. Meade and S. T. Nguyen, *Angew. Chem., Int. Ed.*, 2010, **49**, 9960–9964.
4 W. H. Chiang, W. C. Huang, C. W. Chang, M. Y. Shen, Z. F. Shih, Y. F. Huang, S. C. Lin and H. C. Chiu, *J. Controlled Release*, 2013, **168**, 280–288.
5 W. Wang, D. Cheng, F. M. Gong, X. M. Miao and X. T. Shuai, *Adv. Mater.*, 2012, **24**, 115–120.
6 Y. Li, G. H. Gao and D. S. Lee, *Adv. Healthcare Mater.*, 2013, **2**, 388–417.
7 W. Chen, F. H. Meng, R. Cheng and Z. Y. Zhong, *J. Controlled Release*, 2010, **142**, 40–46.
8 Q. Yan, J. Y. Yuan, Z. N. Cai, Y. Xin, Y. Kang and Y. W. Yin, *J. Am. Chem. Soc.*, 2010, **132**, 9268–9270.
9 H. C. Chiu, Y. W. Lin, Y. F. Huang, C. K. Chuang and C. S. Chern, *Angew. Chem., Int. Ed.*, 2008, **47**, 1875–1878.
10 W. C. Huang, W. H. Chiang, S. J. Lin, Y. J. Lan, H. L. Chen, C. S. Chern and H. C. Chiu, *Adv. Funct. Mater.*, 2012, **22**, 2267–2275.
11 Y. F. Huang, W. H. Chiang, P. L. Tsai, C. S. Chern and H. C. Chiu, *Chem. Commun.*, 2011, **47**, 10978–10980.
12 S. Fujii, Y. Sanada, T. Nishimura, I. Akiba, K. Sakurai, N. Yagi and E. Mylonas, *Langmuir*, 2012, **28**, 3092–3101.
13 Y. L. Chiu, S. C. Chen, C. J. Su, C. W. Hsiao, Y. M. Chen, H. L. Chen and H. W. Sung, *Biomaterials*, 2009, **30**, 4877–4888.
14 I. Hoffmann, P. Heunemann, S. Prevost, R. Schweins, N. J. Wagner and M. Gradzielski, *Langmuir*, 2011, **27**, 4386–4396.
15 B. J. Heuser, M. M. C. Allain and W. C. Chen, *Phys. Rev. B: Condens. Matter Mater. Phys.*, 2002, **66**, 155419.
16 M. Kroon, W. L. Vos and G. H. Wegdam, *Int. J. Thermophys.*, 1998, **19**, 887–894.
17 A. J. Cole, V. C. Yang and A. E. David, *Trends Biotechnol.*, 2011, **29**, 323–332.
18 J. V. Jokerst and S. S. Gambhir, *Acc. Chem. Res.*, 2011, **44**, 1050–1060.
19 J. Xie and S. Jon, *Theranostics*, 2012, **2**, 122–124.
20 P. B. Santhosh and N. P. Ulrih, *Cancer Lett.*, 2013, **336**, 8–17.
21 C. Paquet, H. W. de Haan, D. M. Leek, H. Y. Lin, B. Xiang, G. Tian, A. Kell and B. Simard, *ACS Nano*, 2011, **5**, 3104–3112.
22 W. H. Chiang, V. T. Ho, H. H. Chen, W. C. Huang, Y. F. Huang, S. C. Lin, C. S. Chern and H. C. Chiu, *Langmuir*, 2013, **29**, 6434–6443.
23 K. E. Lokling, R. Skurtveit, A. Bjornerud and S. L. Fossheim, *Magn. Reson. Med.*, 2004, **51**, 688–696.
24 D. Lindner and D. Raghavan, *Br. J. Cancer*, 2009, **100**, 1287–1291.

Published on 12 June 2014. Downloaded by National Tsing Hua University on 29/07/2014 02:52:51.

This journal is © The Royal Society of Chemistry 2014